Generation of Microparticles Using CO_2 and CO_2-Philic Antisolvents

Marazban Sarkari, Inaas Darrat, and Barbara L. Knutson
Dept. of Chemical and Materials Engineering, University of Kentucky, Lexington, KY 40506

Precipitation using a compressed antisolvent (PCA) is a demonstrated technology for generation of monodisperse ultrafine particles. Microparticle precipitation using CO_2-philic antisolvents was studied with the ultimate goal of developing fundamental approaches to tailor microparticle generation. The ability to micronize small solutes and polymeric systems using CO_2-philic liquid antisolvents is compared to precipitation with compressed CO_2 and traditional antisolvents. Analogies are made between PCA and CO_2-philic antisolvent precipitation based on thermodynamic driving forces and the dynamics of the spray process. Analysis of the interfacial gradient energies of the miscible solvent–antisolvent systems indicates that the spray process is dominated by turbulent mixing and not atomization. The similar microparticle morphologies of amorphous and semicrystalline poly(lactic acid) (PLA) obtained using liquid CO_2-philic antisolvents and compressed CO_2 suggest that a similar demixing mechanism dominates microparticle formation at these operating conditions.

Introduction

Ultrafine particles are finding increasing applications in the manufacture of advanced ceramic materials, pigments, catalysts, coatings, microsensors, and the formulation of injectables, inhalables, and controlled release pharmaceuticals. Each application requires monodisperse particles of a specific size, size distribution, composition, and morphology. A variety of mechanical and nonmechanical particle–generation options exist (reactions with aerosols, fluid grinding, spray drying, solvent evaporation, lyophilization, emulsion polymerization, and nonsolvent addition). However, no single technique is capable of meeting size and morphology requirements across all solute systems. This is particularly true of microparticle formation techniques for pharmaceutical applications, where variation of size, purity, and stability must be minimized while maintaining desirable powder–flow properties.

Antisolvent precipitation from droplets using compressed or supercritical CO_2 is a demonstrated alternative technology to existing microparticle generation techniques. This versatile technique has been applied to the generation of a range of ultrafine particles, including pigments, pharmaceuticals, biologically active proteins, biodegradable polymers, catalysts, superconductor precursors, and explosives (Bodmeier et al., 1995; Winters et al., 1996; Reverchon, 1999). Additional useful morphologies, such as nanoparticles, microballoons, microfibers, crystals, and multiple-solute microencapsulations, have been achieved using compressed antisolvents (Dixon et al., 1993; Luna-Bárcenas et al., 1995; Young et al., 1999). The desirable size (usually 1–5μm), narrow size distribution, high yields, and high purity of particles produced using compressed antisolvents address many of the disadvantages of existing technologies.

The process of contacting a compressed antisolvent and a dissolved solute by spraying is known by various acronyms including PCA (precipitation with a compressed antisolvent) (Dixon et al., 1993) and SAS (supercritical antisolvent precipitation) (Yeo et al., 1993). The benefits of PCA, which generally employs liquid or supercritical CO_2 as the antisolvent, are based on both the nature of the compressed antisolvent and the choice of solvent. Temperature and pressure can be used to manipulate the solvent strength of a compressed fluid, particularly near the critical point, and provide a means to vary particle size and morphology. Additionally, solvent-free products are obtained from compressed antisolvent processes following system depressurization. Supercritical CO_2 (T_c =

Correspondence concerning this article should be addressed to B. L. Knutson.

31.1°C, $P_c = 73.8$ bar) as a process solvent offers the additional benefits of being nonflammable, nontoxic, environmentally acceptable, inexpensive, and possessing a mild critical temperature suitable for the processing of thermally labile compounds.

The unique morphologies of PCA-produced particles are generally attributed to the high supersaturations that are achieved in compressed or supercritical CO_2 relative to traditional liquid antisolvents (Randolph et al., 1993; Mawson et al., 1997a). The solvent droplets containing the dissolved solute(s), when sprayed into a CO_2 continuum, are simultaneously evaporated into CO_2 and expanded by CO_2, leading to solute precipitation. In spite of the versatility of PCA as a microparticle-generation technique, the fundamentals of this process are not well understood. This lack of understanding is confounded by the conflicting trends that have been observed for the variation of particle size with PCA processing conditions, as recently summarized by Reverchon (1999). For example, an increase in density (or pressure) at constant temperature has been reported to decrease particle size (Bodmeier et al., 1995), increase particle size (Randolph et al., 1993), or have no detectable effect on particle size (Schmitt et al., 1995).

Approaches to interpreting particle morphology as a function of PCA processing variables recognize the significance of both thermodynamics and mass transfer in the atomized droplet. Variations in microparticle structures have been described by inferring the phase region of precipitation from mass-transfer pathways on ternary polymer–solvent–CO_2 phase diagrams (such as Dixon et al., 1993; Mawson et al., 1997b). Particle morphology has also been interpreted based on nucleation and the subsequent growth of the particles (Winters et al., 1996; Mawson et al., 1997a). In addition, jet breakup and atomization in the spray process has been suggested as a controlling factor in PCA precipitation (Dixon et al., 1994). The balance of thermodynamic and kinetic forces that drive the precipitation process is difficult to examine directly in pressurized systems. However, there exists the possibility of studying these mechanisms indirectly through the examination of alternative nonpressurized antisolvents.

Two significant trends in compressed CO_2 technology suggest that alternative solvents at atmospheric pressure can be used to obtain microparticles similar to PCA-produced particles. First, many of the precipitation processes in CO_2 actually occur at liquid, not supercritical conditions (such as Mawson et al., 1997a). Second, the nature of CO_2 solvation is currently recognized to be neither lipophilic nor hydrophilic, but has been described as CO_2-philic (DeSimone et al., 1992; Harrison et al., 1996; Fink et al., 1999). The affinity of CO_2 for functionalities such as fluorinated hydrocarbons, fluoroethers, and siloxanes, has been attributed to similar low dielectric constants (ϵ) and low polarizability volumes (α) (O'Shea et al., 1991; Diep et al., 1998). Favorable specific intermolecular interactions between CO_2 and the fluorinated solutes have also been proposed (such as DeSimone et al., 1992; O'Neill et al., 1998).

This work examines two commercially available solvents that comprise CO_2-philic functionalities, a hydrofluoroether and a highly fluorinated hydrocarbon, as antisolvents for the generation of ultrafine particles. The microparticle generation and coprecipitation of the model pharmaceutical compounds, poly(L-lactic acid) (L-PLA), poly(DL-lactic acid) (DL-PLA), and griseofulvin (GF), using liquid CO_2-philic antisolvents, are examined. The resulting particles are compared to those obtained by PCA as well as traditional liquid nonsolvents, and the results are interpreted based on thermodynamic driving forces, measures of solvent strength, and solvent-dependent characteristics of the spray contacting process. The success of ultrafine particle generation with CO_2-philic liquids suggests their importance as tools for the fundamental study of CO_2-based precipitation processes without the experimental complications of pressure as well as their commercial potential.

Materials and Methods

Materials

L-PLA (MW 100 kDa) and DL-PLA (MW 15-25 kDa) were purchased from Polysciences Ltd. Griseofulvin (> 95%), perfluorohexane (99%), methylene chloride (> 99.8%), chloroform (99.9%), hexane (99.9%), and ethanol (HPLC grade) were obtained from Sigma. HFE-7100 (3M Specialty Fluids) is an approximately equimolar mixture of two isomers, methoxy-nonafluoroisobutane and methoxy-nonafluorobutane, with essentially identical properties according to product literature. Vertrel (1,1,1,2,3,4,4,5,5,5-decafluoropentane) is a product of DuPont. The probes for determining π^* for the fluorinated solvents [2-nitroaniline (98%), 3-nitroaniline (98%), and 3,5-dinitroaniline (97%)] were purchased from Aldrich. Zero-grade CO_2 was obtained from MG Industries (Malvern, PA). All the solutes and solvents were used without further purification.

Particle generation

Precipitation of pure and codissolved solutions of L-PLA and GF was investigated from two solvents, $CHCl_3$ and CH_2Cl_2. The concentration of pure L-PLA and GF solutions was 7 mg/mL (0.47 wt %). Solutions in which L-PLA and GF were codissolved had a total concentration of 10 mg/mL (0.68 wt %) with the L-PLA/GF ratio set at 9:1, 7:3, 1:1, and 1:9 (w/w).

Two independent apparatus were used for the pressurized experiments (Figure 1) and nonpressurized experiments (Figure 2). In the pressurized apparatus, the precipitation chamber was a high-pressure view cell (Jerguson 16TM-40, ~ 42 mL, rated to 345 bar) placed in a controlled-temperature air bath. Pressurized experiments were conducted by spraying the solution of GF, L-PLA, or a fixed ratio of the two in either $CHCl_3$ or CH_2Cl_2 through a 30-cm-long capillary of either 30-, 50-, or 100 μm diameter into a continuum of cocurrently flowing liquid or supercritical CO_2. The organic solution was sprayed using an ISCO 260D pump at rates ranging from 0.2 mL/min to 3.0 mL/min for 15–30 min. The pressure in the precipitation chamber was maintained by flowing CO_2 using an ISCO 500D syringe pump. The CO_2 flow rate was adjusted to 10–15 mL/min using an Autoclave micrometering valve (10VRMM2812). Microparticles were removed from the flowing CO_2-expanded organic solution using 2-μm frits (Supelco 5-8264) located at the bottom of the precipitation chamber. All precipitations in liquid CO_2 were conducted at 25°C and 67.1 bar, while those in supercritical CO_2 were at

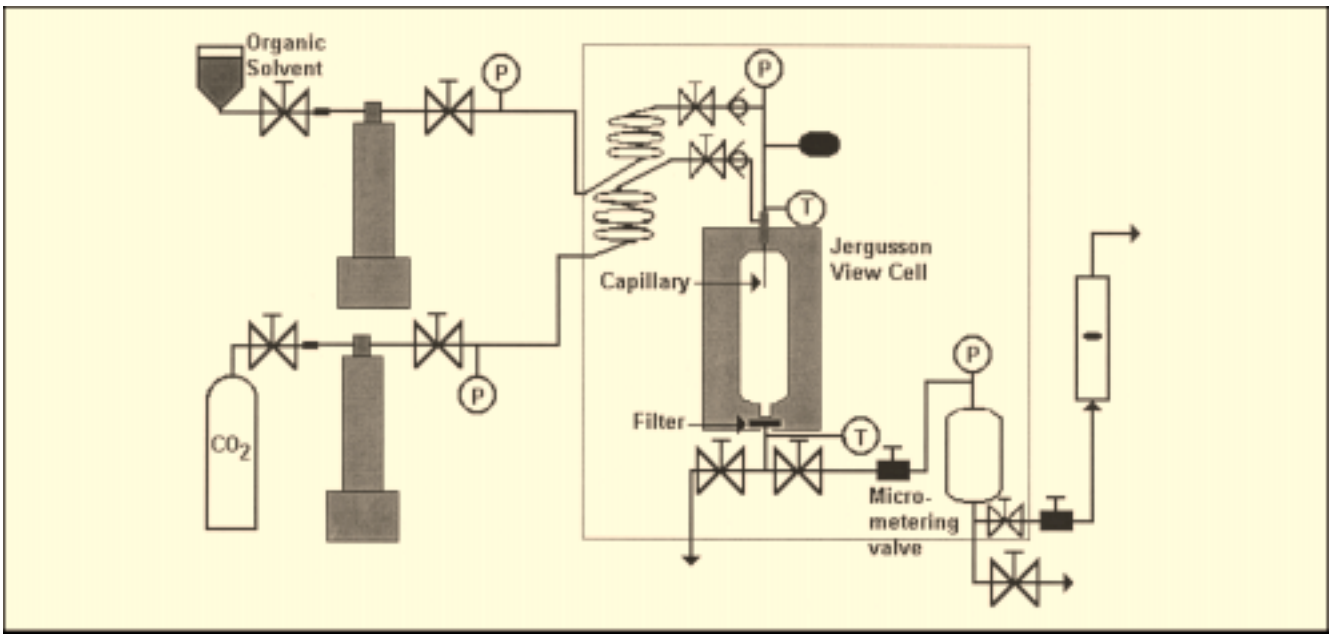

Figure 1. Pressurized spray system.

36°C and 101.1 bar. At these flow rates and conditions, steady-state concentrations of solvent in the outlet ranged from 3 wt. % to 20 wt. %. After spraying, the precipitate was dried with pure CO_2 at 36°C and 134 bar for 30 min. at ~ 10 mL/min. The particles were recovered from the filter following system depressurization at approximately 25 bar/min.

Atmospheric precipitation experiments were conducted in a jacketed glass column precipitator (Kontes Chromaflex OR, 1-cm internal diameter and 47-mL internal volume) (Figure 2). The column was initially filled with the liquid antisolvent.

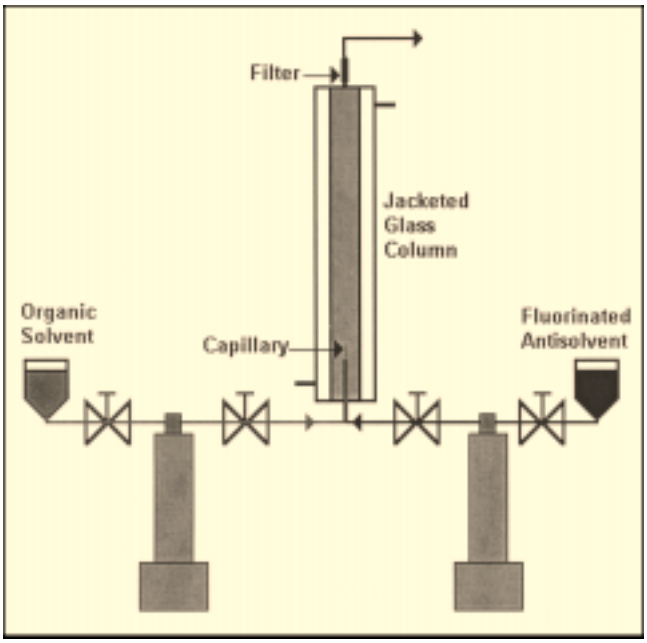

Figure 2. Atmospheric spray system.

The organic solution containing the dissolved model pharmaceuticals was sprayed from the bottom of the precipitation chamber through a 30-cm-long fused silica capillary column (100 μm diameter) into the stationary antisolvent phase maintained at atmospheric pressure and 22°C. The organic solutions were sprayed upward because the particles were lighter than the antisolvent continuum and tended to float toward the top of the column. The solvent solution was sprayed for approximately 2 min at flow rates ranging from 0.3 mL/min to 3.0 mL/min. The maximum wt. % of solvent added to the static antisolvent was 12 wt. %. Following the spray process, the precipitate was collected on an in-line 2-μm filter (Swagelok, SS-2F-K4-2) located at the top of the precipitation chamber by pumping 50 mL of the antisolvent into the bottom of the column. The filter was disassembled to collect the microparticles, which were dry in appearance several seconds after opening the filter.

Determination of π^* values.

The Kamlet-Taft π^* scale of solvent dipolarity is widely used to compare and predict solvent interactions. Solvatochromic probes have been used to quantify π^* for compressed solvents (Lagalante et al., 1998) as well as traditional liquid solvents. The π^* values of HFE-7100 and Vertrel were determined from spectroscopic measurements based on the following system of probe molecules: 2-nitroaniline, 3-nitroaniline, and 3,5-dinitroaniline (Kamlet et al., 1983). The wavelength of the spectral peak of maximum absorbance corresponding to the $\pi \rightarrow \pi^*$ electronic transition for each solute was measured using a UV spectrophotometer (Spectronic Genesys 5, reproducible to ± 0.2 nm). The concentration of the solutes was approximately 10^{-5} M.

These solutes are nonhydrogen bonding and hence the following simplified equation was used to calculate the π^* val-

Table 1. Particle Morphologies as a Function of Solute/Antisolvent Systems

Antisolvent	Solute	Mean Particle Size (μm)	Description
CO_2 (SCF; 36°C, 101.1 bar)		1.06 ± 0.50	Spherical with agglomeration
CO_2 (Liq; 25°C, 67.1 bar)		0.45 ± 0.16	Spherical with agglomeration
HFE-7100	L-PLA	0.78 ± 0.24	Ellipsoid particles
Ethanol		—	Agglomerated precipitate
CO_2(SCF; 36°C, 101.1 bar)		106.7 ± 42.6 (length)	Needle-shaped crystals
		1.27 ± 0.41 (width)	
HFE-7100		46.6 ± 4.7 (length)	Plate-like crystals
	GF	9.4 ± 0.61 (width)	
Hexane		141.8 7 ± 58.0 (length)	Needle-shaped crystals
		3.00 ± 1.52 (width)	
CO_2 (SCF; 36°C, 101.1 bar)		1.04 ± 0.48	Spherical with agglomeration
CO_2 (Liq; 25°C, 67.1 bar)		0.64 ± 0.29	Spherical
HFE-7100	GF + L-PLA	0.30 ± 0.08	Spherical with agglomeration
Vertrel	(1:9 wt ratio)	4.15 ± 1.4	Spherical with a flaky surface
HFE-7100	DL-PLA	0.52 ± 0.23	Spherical with agglomeration

ues of the fluorinated antisolvents (Lagalante et al., 1998):

$$\pi^* = \frac{\nu_{max} - \nu_0}{s}, \quad (1)$$

where ν_{max} and ν_0 are the wave number for absorbance maximum in the solvent and in cyclohexane (the reference solvent), respectively. The susceptibility constant, s, is a measure of the sensitivity of the $\pi \rightarrow \pi^*$ transition to solvent polarity effects. It is indicative of the stability of the ground state of the solute with respect to the excited state (O'Neill et al., 1993). The values for ν_0 and s were obtained from Kamlet et al. (1977). The data reported are averaged values from triplicate measurements for each solute. A simple arithmetic average over solutes was used to obtain the solvent π^* value. To verify the accuracy of our technique, the π^* of hexane was also determined to be -0.07 ± 0.04, which compared well to the literature value of -0.081 (Kamlet et al., 1977).

SEM analysis

The precipitates were mounted on aluminum stubs using double-adhesive carbon-conductive tabs (Ted Pella, Inc.) and coated with Ni in an Emscope SC400 sputter-coater under an Ar atmosphere. A Hitachi S-3200N scanning electron microscope (SEM) at an accelerating voltage of 10 kV with a secondary electron detector was used to obtain digital images of the samples. The particle sizes reported in Table 1 were measured from the SEM images using image analysis software (Quartz PCI). The values reported are the average diameters measured for 100 individual particles.

Results and Discussion

Microparticle formation and characterization

The ability to achieve the high supersaturations that result in monodisperse microparticulates has been attributed to thermodynamic, kinetic, and droplet atomization processes that are unique to compressed and supercritical antisolvents, particularly CO_2. The contribution of these fundamental processes to the generation of ultrafine particles by PCA is examined in this work by using liquid antisolvents that share many solvent features with liquid CO_2. CO_2-philic solvents (HFEs, HFCs, perfluorocarbons, and volatile methylsiloxanes) are characterized by low surface tensions (Gaines et al., 1991), which promote droplet breakup and mixing, and low liquid cohesive energy densities, a measure of solvent strength (Table 2). Furthermore, the viscosity of these CO_2-philic solvents is relatively low. The low heat of vaporization and high vapor pressure of these CO_2-philic solvents facilitates the complete removal of solvent and subsequent solvent recovery.

Intuitively, perfluorohexane would be a representative CO_2-philic antisolvent because of its fluorocarbon groups. It has also been suggested as a good model solvent to test for solute solubility in supercritical CO_2 (Iezzi et al., 1989). Solubility experiments demonstrated its immiscibility with the commonly used organic solvents, making it a poor choice of

Table 2. Selected Physical Properties of the Antisolvents

Antisolvent	Density (kmol/m^3)	Surface Tension (N/m)	Viscosity (Pa·s)	δ (MPa)$^{0.5}$	π^*	$\alpha/V^\dagger$ $\times 10^{-3}$
CO_2 (SCF; 36°C, 101.1 bar)	705.8		$\sim 5.50 \times 10^{-5}$	11.50	-0.25^*	26.1
CO_2 (Liq; 25°C, 67.1 bar)	712.8	5.69×10^{-4}	6.38×10^{-5}	14.56	-0.15^*	27.0
Perfluorohexane	1,669	1.20×10^{-2}	6.68×10^{-4}	12.10	-0.40^{**}	36.9
HFE-7100	1,496	1.36×10^{-2}	6.10×10^{-4}	13.54	0.21 ± 0.03	37.0
Vertrel	1,580	1.41×10^{-2}	6.70×10^{-4}	13.67	0.43 ± 0.11	44.0
Ethanol	787.3	2.20×10^{-2}	1.08×10^{-3}	26.42	0.54^{**}	52.6

*From Sigman et al. (1985).
**From Kamlet et al. (1983).
†Calculated from Miller and Savchik (1979).

antisolvent. In contrast, a range of organic solvents, including $CHCl_3$, CH_2Cl_2, ethanol, and methanol, are highly soluble in compressed CO_2, HFE-7100, and Vertrel.

Ultrafine particle generation by compressed CO_2 and the CO_2-philic antisolvents, HFE-7100, and Vertrel, is demonstrated for several solutes precipitated from $CHCl_3$, or CH_2Cl_2 solutions. Table 1 summarizes the morphology of GF, L-PLA, and DL-PLA precipitates and GF/L-PLA coprecipitates generated from compressed CO_2, CO_2-philic antisolvents, and the traditional liquid antisolvents, ethanol and hexane. L-PLA and GF were chosen as model solutes based on the potential applications of their respective microparticles and their low solubilities in CO_2 (Tom and Debenedetti, 1991; Reverchon et al., 1995). L-PLA is an FDA approved biodegradable polymer used in numerous PCA studies, partly because it is semicrystalline, minimizing its plasticization by CO_2. GF is an antifungal drug that has an increase in bioavailability upon micronization (Reverchon et al., 1995).

L-PLA microparticles generated using liquid and supercritical CO_2 are similar in size and morphology (Figure 3a and 3b). The particles are spherical, slightly agglomerated, and within the size range 0.5–2.5 μm. These L-PLA particles are of similar sphericity and size as those obtained by Randolph et al. (1993) and Bodmeier et al. (1995) by spraying into liquid and supercritical CO_2. Further, the trend of increasing particle size with increase in operating temperature (Table 1) is similar to that observed by these research groups. No difference was found in particles precipitated from $CHCl_3$ and CH_2Cl_2. The precipitation of L-PLA from $CHCl_3$ using HFE-7100 as the antisolvent produced microparticles of a comparable morphology to PCA-processed microparticles

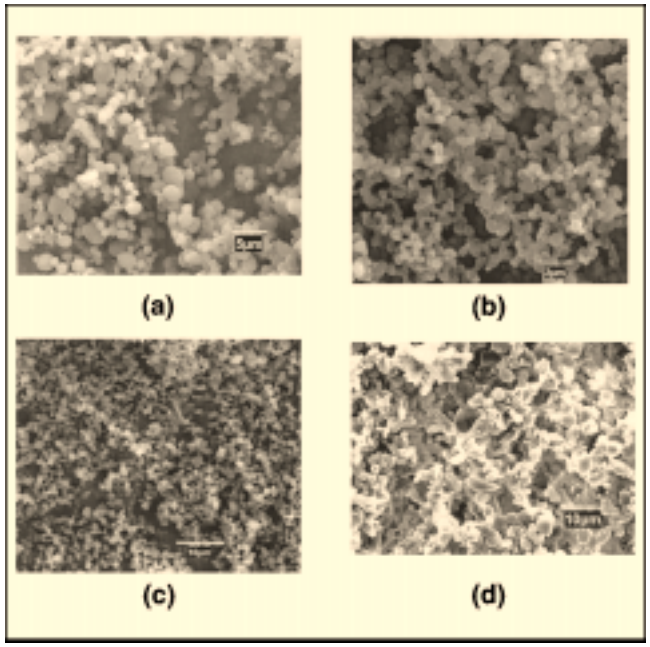

Figure 3. L-PLA dissolved in $CHCl_3$ sprayed into: (a) cocurrently flowing supercritical CO_2 (36°C, 101.1 bar); (b) cocurrently flowing liquid CO_2 (25°C, 67.1 bar); (c) static HFE-7100 (22°C); (d) static ethanol (22°C).

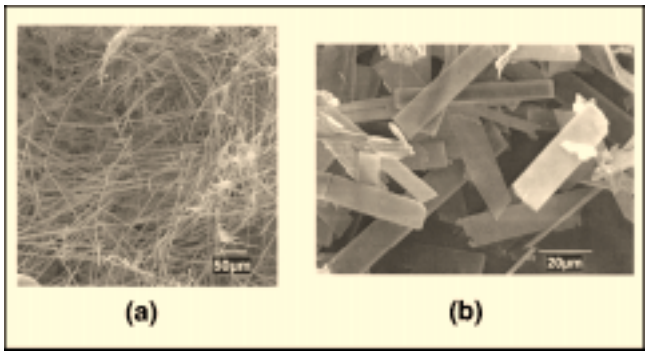

Figure 4. GF dissolved in $CHCl_3$ sprayed into: (a) cocurrently flowing supercritical CO_2 (36°C, 101.1 bar); (b) static HFE-7100 (22°C).

(Figure 3c). The size of the particles precipitated from HFE-7100 is intermediate to that obtained in liquid and supercritical CO_2. As in PCA experiments, precipitation from the spray appeared to be instantaneous. This is in contrast to precipitation with a traditional nonsolvent (ethanol), where a less intense jet breakup and an observable delay in precipitation were apparent for droplets of L-PLA precipitated from $CHCl_3$. The resulting morphologies are distinct from those obtained by spraying into CO_2 and CO_2-philic solvents, as shown in Figure 3d. The polymer is highly agglomerated and has little fine structure.

Precipitates of GF in supercritical CO_2 and HFE-7100 are shown in Figure 4a and 4b, respectively. The precipitate obtained in supercritical CO_2 was a light voluminous powder comprising large needle-like crystals of GF, a morphology also observed by Reverchon et al. (1995). The longer axis of these particles is about two orders of magnitude larger than the width. The compacted powder obtained after precipitation from HFE-7100 showed large broken platelike crystals of GF. The use of hexane as a nonsolvent yielded precipitates similar to those obtained in CO_2. Vertrel and ethanol could not be used as antisolvents for GF because of the comparatively high solubility of GF in these solvents (0.34 mol fraction in Vertrel and 0.32 mol fraction in ethanol).

The coprecipitation of pharmaceuticals and biodegradable polymers has been achieved in previous PCA investigations (Bodmeier et al., 1995; Falk and Randolph, 1998). Therefore, an antisolvent system comparable to compressed CO_2 should also be capable of precipitating codissolved solutes of similar morphologies. Coprecipitates of GF and L-PLA using supercritical CO_2 and HFE-7100 as antisolvents are shown in Figure 5a and 5b, respectively, at a L-PLA/GF weight ratio of 9:1. For both antisolvent systems, varying the L-PLA/GF weight ratio (9:1, 7:3, 1:1) at constant overall weight percent of solutes did not change the morphology of the particles significantly. At high ratios of L-PLA/GF, the morphology of microparticles generated from both antisolvents is characteristic of the polymer. However, precipitates formed in HFE-7100 using a L-PLA/GF ratio of 1:9 showed needle-like crystals of GF surrounded by L-PLA particles, indicating that this concentration of L-PLA was insufficient to completely coat the GF particles (Figure 5c). A similar change in morphology with drug concentration was noted by Bodmeier et al. (1995)

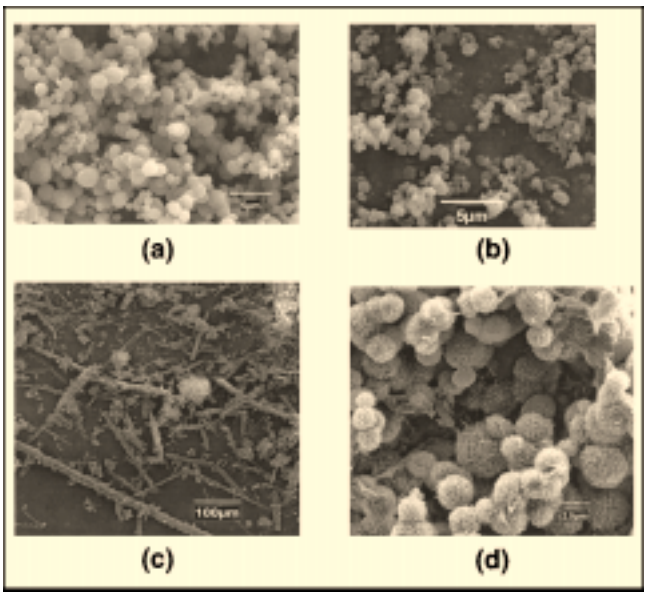

Figure 5. (a) L-PLA/GF (9:1) dissolved in CH_2Cl_2 coprecipitated in cocurrently flowing supercritical CO_2 (36°C, 101.1 bar); (b) L-PLA/GF (9:1) dissolved in $CHCl_3$ coprecipitated into static HFE-7100 (22°C); (c) L-PLA/GF (1:9) dissolved in CH_2Cl_2 coprecipitated into static HFE-7100 (22°C); (d) L-PLA/GF (9:1) dissolved in $CHCL_3$ coprecipitated into static Vertrel (22°C).

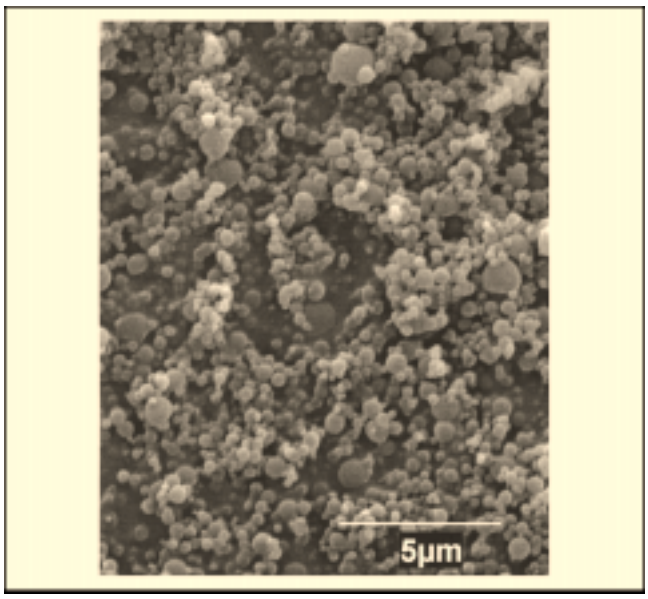

Figure 6. DL-PLA dissolved in $CHCl_3$ sprayed into static HFE-7100 (22°C).

for chlorpheniramine maleate and indomethacin with L-PLA. L-PLA/GF (weight ratio, 9:1) coprecipitates formed from droplets of $CHCl_3$ contacted with Vertrel were in the size range 1.0–7.0 μm (Figure 5d). The distinctly porous structure of these coprecipitated microparticles, which indicates a high surface area, is characteristic of pure L-PLA microparticles precipitated with Vertrel (not shown). These structures can be attributed to the weak antisolvent properties of Vertrel for this solute/solvent system, in which the delay of precipitation was observable relative to that in CO_2 and HFE-7100.

Preliminary investigations on the extent of GF microencapsulation were carried out in acetonitrile, which dissolves GF but not L-PLA. The rate of change in GF concentration was determined spectrophotometrically at 291 nm. The dissolution of pure GF precipitates (from CO_2 or HFE-7100 antisolvent processes) in acetonitrile was instantaneous, which is consistent with the small particle size observed in the SEMs. The initial GF dissolution rate from coprecipitates of L-PLA/GF was $\sim 0.24\times10^{-3}$ mg/mL·h, with complete dissolution of GF from a 2.1-mg sample achieved in 2 h. The slow dissolution rate of GF from L-PLA/GF coprecipitates is consistent with the partial entrapment of GF in the L-PLA matrix.

The ability of compressed CO_2 to plasticize most amorphous polymers precludes its use for generating microparticles of amorphous polymers, such as DL-PLA. Antisolvent precipitation by HFE-7100, a much larger molecule, presents a unique opportunity to create amorphous polymeric microparticles under conditions of reduced plasticization. The slightly agglomerated particles of DL-PLA precipitated from $CHCl_3$ by HFE-7100 are spherical with a diameter of about 0.5 μm (Figure 6). They are strikingly similar to the semicrystalline L-PLA particles generated from HFE-7100, liquid CO_2, and supercritical CO_2. The similarity of the particle morphology suggests a common mechanism of precipitation, one that is not dominated by crystallization. This is consistent with observation that, although crystallization may be thermodynamically favorable, the kinetically favored liquid–liquid demixing process often dominates the resulting polymer morphology, even for rapidly crystallizing polymers such as L-PLA (van de Witte et al., 1996). However, the precipitation mechanism is difficult to evaluate directly from crystallinity because of the potential for solvent or CO_2-induced crystallization (Lambert and Paulaitis, 1991) over the course of the PCA process or the possibility that rapid crystallization followed liquid–liquid demixing to lock in the morphology of the particle.

Compressed CO_2 and CO_2-philic antisolvents appear to provide a unique environment for the formation of L-PLA microparticles relative to traditional liquid antisolvents such as hexane or ethanol. Both HFE-7100 and Vertrel produced polymeric microparticles and coprecipitates with distinct morphologies, whose size ranges were of the same order of magnitude as those formed by CO_2. In contrast, CO_2-philic antisolvents did not produce unique microparticles of the small solute molecule, GF, relative to traditional antisolvents. These results suggest the need for different fundamental treatments of small solutes and polymeric systems in rapid antisolvent processes.

Phase equilibria

The thermodynamic behavior of the binary solvent-compressed CO_2 system has also been used to interpret the microparticles produced by PCA. The volumetric expansion of an organic solvent by CO_2 at conditions where two phases

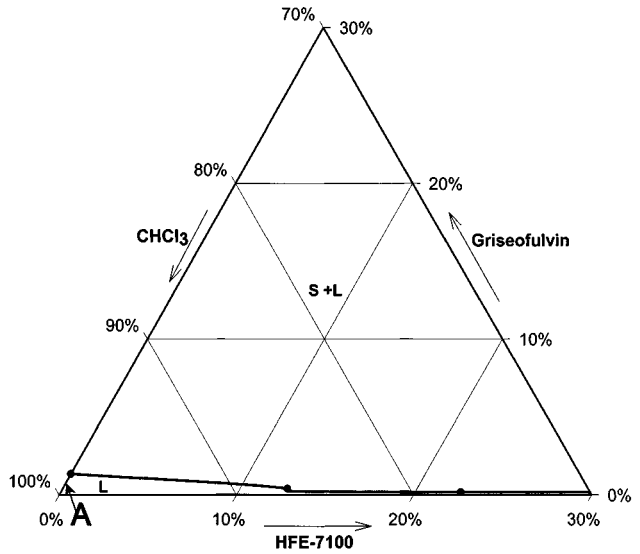

Figure 7. Three-component phase diagram for GF-HFE-7100-$CHCl_3$ system at 22°C.

exist is a measure of the solubility of CO_2 in the solvent. The reduction of solvent strength due to solvent expansion by CO_2 has been qualitatively related to the supersaturation of solutes in the solvent droplets formed by PCA (Reverchon, 1999). However, PCA is most frequently operated at conditions of complete miscibility of the organic solvent and compressed CO_2. Similarly, $CHCl_3$ and HFE-7100 are completely miscible at the operating temperature of this investigation.

Phase equilibria for the ternary system of GF, $CHCl_3$, and HFE-7100 were measured to provide a description of the thermodynamic driving forces of precipitation (Figure 7). Point A in Figure 7 represents a typical initial concentration of GF-$CHCl_3$ solution for the generation of microparticles using HFE-7100. The phase diagram highlights the desirable antisolvent properties of HFE-7100 for this solute/solvent system. It is infinitely miscible with the solvent $CHCl_3$ and does not dissolve the solute GF to any detectable extent. However, an additional separation process would be required to regenerate the organic solvent and antisolvent for reuse. This is in contrast to PCA, where the solvent and antisolvent are easily recoverable with system depressurization. These phase equilibria were easy to determine relative to pressurized experiments representative of PCA, demonstrating the utility of atmospheric CO_2-philic solvents in investigating fundamental phenomena.

Although equilibrium phase diagrams are useful in determining appropriate solute/solvent/antisolvent systems, knowledge of the supersaturation of the solute in the organic-rich droplets is also necessary to interpret microparticle morphology. For example, supercritical CO_2, HFE-7100, and hexane are appropriate antisolvents for GF based on the low solubility of GF in these systems [1.6×10^{-5} mol fraction in CO_2 at 200 bar and 50°C (Reverchon et al., 1995); 10^{-3} mol fraction in HFE-7100 at 25°C and 1 bar; 3.5×10^{-3} mol fraction in hexane at 25°C and 1 bar]. The variation of GF particle morphology with choice of antisolvent cannot be related directly to the solubility of GF or the contacting scheme. HFE-7100 produced precipitates distinctly different from the needle-like structures formed with both CO_2 and hexane (Table 1). However, the solubility of GF in HFE-7100 is intermediate to the other antisolvents. In addition, the method of contacting dissolved GF with the HFE-7100 and hexane was identical. Further examination of kinetic and mass-transfer processes that impact crystallization are warranted.

Analysis of the spray process

Parameters of the spray contacting process, such as the flow rates of the solvent and antisolvent solutions and the nozzle diameter, affect the morphology of PCA-generated particles (Dixon et al., 1993). The Weber number, *We*, a dimensionless quantity that describes the ratio of the dynamic pressure by inertia to the internal pressure by surface tension (Wagner and Eggers, 1996), is a fundamental quantity used to compare atomization processes as a function of spray conditions. *We* is defined as

$$We = \frac{\rho_A V^2 D}{\sigma}, \tag{2}$$

where ρ_A is the antisolvent density, V is the velocity of the jet, D is the droplet diameter, and σ is the interfacial tension. The quantities describing *We*, particularly the interfacial tension, are time-dependent. The interfacial tension is a function of the varying concentration within the droplet. For completely miscible systems, in the absence of a solute, the interfacial tension of the solvent/antisolvent droplet will vanish at equilibrium. Thus, interpretations of PCA microparticle size are based on the initial spray conditions assuming an initial droplet diameter (such as the capillary diameter) and a nonzero interfacial tension.

In this analysis, an interfacial gradient energy for the initial spray conditions was estimated for the miscible solvent/antisolvent systems on the basis of density-gradient theory (Cahn and Hilliard, 1958). The theory considers the interface to be a nonuniform region whose composition varies continuously between that of the two pure phases. It has been used to describe the equilibrium surface tensions of pure components and the interfacial tension of immiscible liquids. In addition, density-gradient theory has been extended to calculate the excess energy of the transient interface for the mixing of two miscible fluids (Smith et al., 1981). The interfacial tension is related to the gradient energy across the interface as follows:

$$\sigma = \int_0^L \left(\Delta G(\rho) + \sum_{i,j} C_{ij} \frac{d\rho_i}{dx} \frac{d\rho_j}{dx} \right) dx, \tag{3}$$

where $\Delta G(\rho)$, the difference in free energy of the actual system and that if it was completely homogeneous; C_{ij} are the ''influence parameters'' for the components i and j and can be evaluated from statistical mechanical considerations; and ρ_i and ρ_j are the local densities of the components i and j, respectively. The integration is performed as a function of x, the direction perpendicular to the interface, over the distance of the gradient, L.

The contribution of the total free energy of the interface relative to the chemical potentials of each species at their

respective equilibrium states for a binary system is

$$\sigma_1 = \int_0^L \left[\rho_A \left(\mu_A - \mu_A^0 \right) + \rho_B \left(\mu_B - \mu_B^0 \right) \right] dx, \qquad (4)$$

where μ_i and μ_i^0 are the local and reference chemical potentials, respectively, of species i. The variation of the local density across the two-phase system contributes to the interfacial tension of a binary system as follows:

$$\sigma_2 = \int_0^L \left(C_{AA} \left(\frac{d\rho_A}{dx} \right)^2 + C_{BB} \left(\frac{d\rho_B}{dx} \right)^2 + 2C_{AB} \left(\frac{d\rho_A}{dx} \frac{d\rho_B}{dx} \right) \right) dx. \qquad (5)$$

The density-gradient theory was applied to the miscible solvent–antisolvent systems $CHCl_3$/supercritical CO_2, $CHCl_3$/ethanol, and $CHCl_3$/HFE-7100 to estimate the magnitude of the initial *We* number (in the absence of a solute). The composition gradient across the interface was described by a linear profile, which captured the relevant features of the interfacial events in miscible systems during the spray process. The mol fraction of the antisolvent at the $CHCl_3$ boundary increased from 0.1 to 0.85, while at the antisolvent-rich boundary, it decreased from 0.9 to 0.85. As suggested by Davis (1988), the length of the interface (L) increased proportional to $(Dt)^{1/2}$, where D is the diffusivity of $CHCl_3$ in the antisolvent. The diffusivity of $CHCl_3$ in supercritical CO_2 was estimated from Dariva et al. (1999) to be 1.2×10^{-08} m^2/s. The Wilke-Chang method was used to estimate the diffusivity of $CHCl_3$ in ethanol and HFE-7100 as 2.7×10^{-09} and 2.3×10^{-09} m^2/s, respectively. The initial value of L, L_0, was calculated as the radius of the spherical volume represented by the average solvent–antisolvent b parameter from the Peng-Robinson equation of state (PR EOS). The L_0 values for the $CHCl_3$/supercritical CO_2, $CHCl_3$/ethanol, and $CHCl_3$/HFE-7100 were 0.26 nm, 0.28 nm, and 0.35 nm, respectively, which are similar to the liquid–vapor interfacial thickness for Ar (0.28 nm) reported by Ono and Kondo (1960).

The contribution of chemical potential differences (σ_1) across this linear gradient was calculated as a ratio of the local fugacity relative to a representative single-phase mixture reference fugacity using PR EOS. Since the antisolvent is always present in greater proportion than the solvent, the mixture reference point for all solvent–antisolvent systems was taken as 15 mol % $CHCl_3$. The standard mixing rules as described by Peng and Robinson (1976), with k_{ij} set as 0.1, were used to calculate mixture properties for all the systems. The contribution of the density gradient (σ_2) to the dynamic interfacial tension was also calculated from the antisolvent-dependent linear composition profile. The pure-component interaction values, C_{ii}, are reported for CO_2, ethanol, and $CHCl_3$ as 25.8×10^{-21}, 53.0×10^{-21}, and 179×10^{-21} $J\cdot m^5\cdot mol^{-2}$, respectively (Cornelisse, 1997). The C_{ii} of pure HFE-7100 and Vertrel were estimated from a correlation of $ab^{2/3}$ (a and b being the PR EOS parameters), a format suggested by Zuo and Stenby (1997) for classes of similar fluids. The C_{ii} values of 691×10^{-21}, and 493×10^{-21} $J\cdot mol^5\cdot mol^{-2}$ for HFE-7100 and Vertrel, respectively, were based on a linear plot of the reported values of C_{ii} vs. $ab^{2/3}$ ($r^2 = 0.969$). The cross-interaction parameters, C_{AB}, were calculated as the geometric mean of the respective pure components C_{ii}s (Carey et al., 1980).

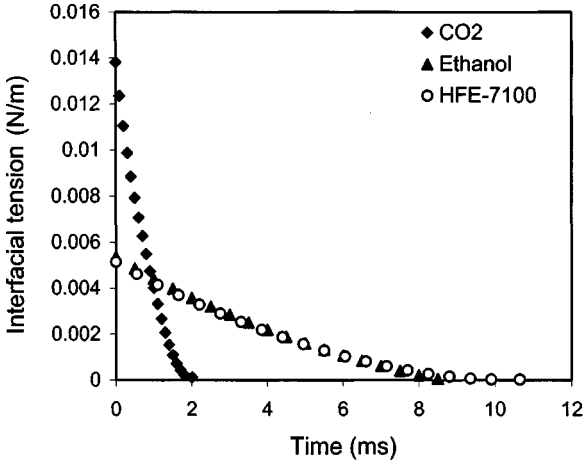

Figure 8. Comparison of time variant σ for supercritical CO_2, ethanol and HFE-7100.

Thus, the total interfacial tension, the sum of σ_1 and σ_2, is given in Figure 8 for the systems of $CHCl_3$/supercritical CO_2 (37°C and 100 bar), $CHCl_3$/HFE-7100, and $CHCl_3$/ethanol as a function of time, assuming a maximum gradient length of 5 μm. Although σ_1 and σ_2 are of the same order of magnitude, σ_1 makes a larger contribution to the total interfacial tension. In all cases, the interfacial energy of these miscible systems tends to zero as the gradient advances. Initial interfacial tensions (calculated over L_0) were 13.8 mN/m, 5.36 mN/m, 5.14 mN/m, and 5.79 mN/m for $CHCl_3$ with supercritical CO_2, ethanol, HFE-7100, and Vertrel, respectively, which are similar in magnitude to 1 mN/m obtained by Smith et al. (1981) for a system of miscible silicone oils. Although the initial value of σ for CO_2 is high relative to the liquid antisolvents, it approaches zero over a shorter time based on its higher diffusivity relative to the liquid antisolvents.

Due to the presence of dissolved solute in the droplet, the interfacial energy gradients are not valid over the range of the precipitation process. However, the initial interfacial energies were assumed to be representative of the spray process and were therefore used to interpret the resulting microparticle morphologies based on initial *We*. *We* was varied from 23 to 850 for a single antisolvent (supercritical CO_2) by changing the capillary diameter at a constant flow rate of 1 mL/min. No statistically significant variation of particle size was observed with change in capillary size. Similarly, the size of the microparticles produced in supercritical CO_2 and HFE-7100 at identical flow conditions (Table 1) did not vary significantly, although the initial *We* for the fluids are 23 and 129, respectively. In contrast, HFE-7100 and Vertrel produced distinctly different L-PLA microparticles (Figures 5c and 5d) at similar *We* (129 and 133, respectively). At the same flow conditions (initial *We* of 66) ethanol did not produce microparticles.

All initial *We* investigated in these miscible solvent–antisolvent systems are greater than the critical *We* (reported to

range between 6 and 50; Bayvel and Orzechowski, 1993), suggesting that the spray process is dominated by turbulent mixing and not droplet formation. This is consistent with the visual examination of the spray process, where droplet formation was not observed in these miscible systems at these flow conditions. A visual examination of a similar PCA spray process by Mawson et al. (1997c) showed an increase in spray intensity and turbulence with increasing organic solution flow rates, and hence increasing *We*. Therefore, for these miscible systems and at these spray conditions, *We* is not an effective predictor of microparticle size.

Solvent characterization

Solvent parameters such as π^*, the polarizability volume (α), and the cohesive energy density (δ) are measures of solvent strength as well as indicators of fundamental solvent properties, such as interfacial tension. The values of these parameters for the antisolvents investigated are examined to provide further understanding of the uniqueness of PCA-produced microparticles relative to atmospheric liquid antisolvent processes.

The π^* scale of solute/solvent polarity has been used to characterize and correlate numerous solvent-dependent properties based on the solvent's ability to stabilize a charge based on its dielectric effect (Kamlet et al., 1997). Table 2 compares the π^* values of the CO_2-philic antisolvents, as measured in our laboratory, with those of compressed CO_2 and the traditional antisolvents. The π^* value of 0.21 for HFE-7100 is similar to that of ethers having a similar number of carbon atoms (such as diisopropyl ether, 0.27; di-*n*-butyl ether, 0.24; diethyl ether, 0.27). This indicates that the ether functional group and the carbon chain length dominate the polarity of HFE-7100. The lower polarity of HFE-7100, however, is consistent with the lower polarizability of the CF_3 and F groups as compared to CH_3 and H (Lagalante et al., 1998).

The measured π^* value of 0.43 for Vertrel, a highly fluorinated hydrocarbon, is more difficult to compare directly, as the only compounds having a similar π^* are aliphatic alcohols (Kamlet et al., 1977). The π^* for Vertrel is higher than that of its aliphatic analog *n*-pentane ($\pi^* = -0.08$) and much higher than that of perfluorinated compounds (such as perfluorohexane, $\pi^* = 0.40$). Lagalante et al. (1998) have reported the values of fluorinated ethanes to range from -1.2 to 0.5 as a function of density and arrangement of the fluorine atoms on the ethane backbone. The high value of 0.43 for Vertrel can be attributed to the acidity of the two hydrogen atoms in proximity to the large number of electronegative fluorine atoms. The negative π^* value of CO_2, obtained from the literature indicates its low polarity. Ethanol has the highest π^* value of all the antisolvents studied. The vast difference in polarities of these antisolvents could indicate their differing interactions with the solutes and organic solvents during precipitation.

An alternative solvent strength parameter, the polarizability volume (α) of a molecule, describes the induced dipole of a molecule as opposed to π^*, which is a measure of the dipolarity of the molecule. Table 2 lists the α/V values for the antisolvents studied, calculated by a group-contribution technique (Miller and Savchik, 1979). The value of α/V increases from CO_2 to the fluorinated antisolvents to the traditional nonsolvents. Of the antisolvents studied, HFE-7100 has an α/V closest to that of CO_2 and also forms particles most like CO_2, suggesting more CO_2- like behavior. Similarly, δ can be directly correlated with surface tension (such as Becher, 1972), and hence the low surface tension fluorinated antisolvents also have low δ values (Table 2). Since interfacial phenomena are critical to spray and crystallization processes, it follows that the δ can correlate with the observed microparticle size. In this investigation, antisolvents with δ values closer to compressed CO_2 (HFE-7100 and Vertrel) form particles similar to those obtained in CO_2.

Characteristic solvent properties such as α/V and δ provide guidelines for the selection of CO_2-philic antisolvents. CO_2-philic solvents possess low α/V and low δ values, indicative of their low surface tension and low viscosities. The utility of CO_2-philic solvents for the precipitation of unique particle morphologies has been demonstrated. However, the applicability of CO_2-philic solvents to specific solute–solvent systems is dictated by phase equilibria, which are related to the intermolecular interactions of the solute–solvent–antisolvent system implied by solvent-strength measures of dipolarity and hydrogen bonding, for example.

Conclusions

A thermodynamic analysis of solute–solvent–antisolvent systems highlights the importance of phase criteria when selecting an antisolvent. The effect of antisolvent choice on microparticle size and morphology cannot be predicted from only phase equilibria, however, as demonstrated by the precipitation of a small crystalline solute (GF) and a polymeric solute (L-PLA) using supercritical CO_2, liquid CO_2, CO_2-philic solvents, and traditional liquid nonsolvents. The size of L-PLA microparticulates precipitated by CO_2-philic antisolvents was similar to those produced by PCA using compressed CO_2. Microspheres of both amorphous and semicrystalline PLA precipitated by the CO_2-philic antisolvent are comparable to PCA-processed semicrystalline L-PLA, suggesting that crystallization is not the dominant demixing mechanism for particle formation. In contrast, the crystalline morphology of the relatively small solute, GF, was a function of antisolvent choice. These results indicate the important contribution of kinetic processes to the uniqueness of PCA-produced microparticles and suggest that different fundamental treatments are required for polymeric solutes relative to low molecular-weight solutes.

An examination of the kinetics of the spray process reveals that turbulent mixing, and not droplet formation, dominates the solvent–antisolvent contacting mechanism in the miscible solvent–antisolvent systems investigated. This result is consistent with both visual observations of the spray process and the relative insensitivity of the microparticle size to the spray conditions over the operating conditions investigated. The ability to generate microparticles and coprecipitates using the CO_2-philic antisolvents HFE-7100 and Vertrel is clearly demonstrated. Antisolvent processing in nonpressurized CO_2-philic liquids represents a significant divergence from current antisolvent processes and presents the opportunity to better understand and control the current PCA process. The ease of experiments using nonpressurized liquid antisolvents

relative to compressed CO_2 indicate the utility of CO_2-philic solvents for fundamental investigations of PCA. For these same reasons, CO_2-philic antisolvents may also have commercial applications.

Acknowledgments

One of the authors (M. S.) gratefully acknowledges the Kentucky Research Challenge Trust Fund for Materials Synthesis for a Graduate Fellowship. The authors are thankful to Larry Rice for assistance with the SEMs.

Literature Cited

Bayvel, L., and Z. Orzechowski, *Liquid Atomization*, Taylor & Francis, Washington (1993).

Becher, P., "The Calculation of Cohesive Energy Density from the Surface Tension of Liquids," *J. Colloid Interface Sci.*, **38**, 291 (1972).

Bodmeier, R., H. Wang, D. Dixon, S. Mawson, and K. Johnston, "Polymeric Microspheres Prepared by Spraying into Compressed Carbon Dioxide," *Pharm. Res.*, **12**, 1211 (1995).

Cahn, J., and J. Hilliard, "Free Energy of a Nonuniform System. I. Interfacial Energy," *J. Chem. Phys.*, **28**, 258 (1958).

Carey, B., L. Scriven, and H. Davis, "Semiempirical Theory of Surface Tension of Binary Systems," *AIChE J.*, **26**, 705 (1980).

Cornelisse, P., "The Gradient Theory Applied Simultaneous Modelling of Interfacial Tension and Phase Behaviour," PhD Thesis, Delft Univ. of Technology, Delft, The Netherlands (1997).

Davis, H., "A Theory of Tension at a Miscible Displacement Front," *Numerical Simulation in Oil Recovery, IMA Volumes in Mathematics and its Applications*, Vol. 11, M. Wheeler, ed., Springer-Verlag, New York, p. 105 (1998).

DeSimone, J., Z. Guan, and C. Elsbernd, "Synthesis of Fluoropolymers in Supercritical Carbon Dioxide," *Science*, **257**, 945 (1992).

Diep, P., K. Jordan, J. K. Johnson, and E. Beckman, "CO_2-Fluorocarbon and CO_2-Hydrocarbon Interactions from First-Principles Calculations," *J. Phys. Chem. A*, **102**, 2231 (1998).

Dixon, D., G. Luna-Bárcenas, and K. Johnston, "Microcellular Microspheres and Microballoons by Precipitation With a Vapor-Liquid Compressed Fluid Antisolvent," *Polymer*, **35**, 3998 (1994).

Dixon, D., K. Johnston, and R. Bodmeier, "Polymeric Materials Formed by Precipitation with a Compressed Fluid Antisolvent," *AIChE J.*, **39**, 127 (1993).

Falk, R., and T. Randolph, "Process Variable Implications for Residual Solvent Removal and Polymer Morphology in the Formation of Gentamycin-Loaded Poly(L-lactide) Microparticles," *Pharm. Res.*, **15**, 1233 (1998).

Fink, R., D. Hancu, R. Valentine, and E. Beckman, "Towards the Development of 'CO_2-philic' Hydrocarbons. 1. Use of Side-Chain Functionalization to Lower the Miscibility Pressure of Polydimethylsiloxanes in CO_2," *J. Phys. Chem. B*, **103**, 6441 (1999).

Gaines, G., Jr., "Surface Activity of Semifluorinated Alkanes: $F(CF_2)_m(CH_2)_nH$," *Langmuir*, **7**, 3054 (1991).

Harrison, K., K. Johnston, and I. Sanchez, "Effect of Surfactants on the Interfacial Tension Between Supercritical Carbon Dioxide and Polyethylene Glycol," *Langmuir*, **12**, 2637 (1996).

Iezzi, A., P. Bendale, R. Enick, M. Turberg, and J. Brady, "'Gel' Formation in Carbon Dioxide—Semifluorinated Alkane Mixtures and Phase Equilibria of a Carbon Dioxide—Perfluorinated Alkane Mixture," *Fluid Phase Equilibr.*, **52**, 307 (1989).

Kamlet, M., J.-L. Abboud, and R. Taft, "The Solvatochromatic Comparison Method. 6. The π^* Scale of Solvent Polarities," *J. Amer. Chem. Soc.*, **99**, 6027 (1977).

Kamlet, M., J.-L. Abboud, M. Abraham, and R. Taft, "Linear Solvation Energy Relationships. 23. A Comprehensive Collection of the Solvatochromatic Parameters, π^*, α, and β, and Some Methods for Simplifying the Generalized Solvatochromic Equation," *J. Org. Chem.*, **48**, 2877 (1983).

Lagalante, A., R. Hall, and T. Bruno, "Kamlet-Taft Solvatochromic Parameters of the Sub- and Supercritical Fluorinated Ethane Solvents," *J. Phys. Chem.*, **102**, 6601 (1998).

Lambert, S. M., and M. E. Paulaitis, "Crystallization of Poly(ethylene terephthalate) Induced by Carbon Dioxide Sorption at Elevated Pressures," *J. Supercrit. Fluids*, **4**, 15, (1991).

Luna-Bárcenas, G., S. Kanakia, I. Sanchez, and K. Johnston, "Semicrystalline Microfibrils and Hollow Fibers by Precipitation with a Compressed-Fluid Antisolvent," *Polymer*, **36**, 3173 (1995).

Mawson, S., K. Johnston, D. Betts, J. McClain, and J. DeSimone, "Stabilized Polymer Microparticles by Precipitation with a Compressed Fluid Antisolvent. 1. Poly(fluoro acrylates)," *Macromol.*, **30**, 71 (1997a).

Mawson, S., S. Kanakia, and K. Johnston, "Metastable Polymer Blends by Precipitation with a Compressed Fluid Antisolvent," *Polymer*, **38**, 2957 (1997b).

Mawson, S., S. Kanakia, and K. Johnston, "Coaxial Nozzle for Control of Particle Morphology in Precipitation with a Compressed Fluid Antisolvent," *J. Appl. Poly. Sci.*, **64**, 2105 (1997c).

Miller, K., and J. Savchik, "A New Empirical Method to Calculate Average Molecular Polarizabilities," *J. Amer. Chem. Soc.*, **101**, 7206 (1979).

O'Neill, M., Q. Cao, M. Fang, K. Johnston, S. Wilkinson, C. Smith, J. Kerschner, and S. Jureller, "Solubility of Homopolymers and Copolymers in Carbon Dioxide," *Ind. Eng. Chem. Res.*, **37**, 3067 (1998).

O'Neill, M., P. Kruus, and R. Burk, "Solvatochromatic Parameters and Solubilities in Supercritical Fluid Systems," *Can. J. Chem.*, **71**, 1834 (1993).

Ono, S., and S. Kondo, "Molecular Theory of Surface Tension in Liquids," *Handbuch der Physik*, Vol. X, *Structure of Liquids*, S. Flügge, ed., Springer-Verlag, Berlin, p. 134 (1960).

O'Shea, K., K. Kirmse, M. Fox, and K. Johnston, "Polar and Hydrogen-Bonding Interactions in Supercritical Fluids. Effects on the Tautomeric Equilibrium of 4-(Phenylazo)-1-Naphthol," *J. Phys. Chem.*, **95**, 7863 (1991).

Peng, D.-Y., and D. Robinson, "A New Two-Constant Equation of State," *Ind. Eng. Chem. Res.*, **15**, 59 (1976).

Randolph, T., A. Randolph, M. Mebes, and S. Yeung, "Sub-Micrometer-Sized Biodegradable Particles of Poly(L-Lactic Acid) via the Gas Antisolvent Spray Precipitation Process," *Biotechnol. Prog.*, **9**, 429 (1993).

Reverchon, E., G. Della Porta, R. Taddeo, P. Pallado, and A. Stassi, "Solubility and Micronization of Griseofulvin in Supercritical CHF_3," *Ind. Eng. Chem. Res.*, **34**, 4087 (1995).

Reverchon, E., "Supercritical Antisolvent Precipitation of Micro- and Nano-particles," *J. Supercrit. Fluids*, **15**, 1 (1999).

Schmitt, W., M. Salada, G. Shook, and S. Speaker, "Finely-Divided Powders by Carrier Solution Injection into a Near or Supercritical Fluid," *AIChE J.*, **41**, 2476 (1995).

Sigman, M., S. Lindley, and J. Leffler, "Supercritical Carbon Dioxide: Behavior of π^* and β Solvatochromic Indicators in Media of Different Densities," *J. Amer. Chem. Soc.*, **107**, 1471 (1985).

Smith, P., T. van de Ven, S. Mason, "The Transient Interfacial Tension Between Two Miscible Fluids," *J. Colloid Inteface Sci.*, **80**, 302 (1981).

Tom, J., and P. Debenedetti, "Particle Formation with Supercritical Fluids—A Review," *J. Aerosol Sci.*, **22**, 555 (1991).

Van de Witte, P., H. Esselbrugge, P. J. Dijkstra, J. W. A. van den Berg, and J. Feijen, "Phase Transitions During Membrane Formation of Polyactides. I. A Morphological Study of Membranes Obtained from the System Polylactide-Chloroform-Methanol," *J. Memb. Sci.*, **113**, 223 (1996).

Wagner, H., and R. Eggers, "Extraction of Spray Particles with Supercritical Fluids in a Two-Phase Flow," *AIChE J.*, **42**, 1901 (1996).

Winters, M., B. Knutson, P. Debenedetti, H. Sparks, T. Przybycien, C. Stevenson, and S. Prestrelski, "Precipitation of Proteins in Supercritical Carbon Dioxide," *J. Pharm. Sci.*, **85**, 589 (1996).

Yeo, S.-D., G.-B. Lim, P. Debenedetti, and H. Bernstein, "Formation of Microparticulate Protein Powders Using a Supercritical Antisolvent," *Biotechnol. Biogen.*, **41**, 341 (1993).

Young, T. J., K. P. Johnston, K. Mishima, and H. Tanaka, "Encapsulation of Lysozyme in a Biodegradable Polymer by Precipitation with a Vapor-over-Liquid Antisolvent," *J. Pharm. Sci.*, **88**, 640 (1999).

Zuo, Y.-X., and E. Stenby, "Calculation of Interfacial Tensions with Gradient Theory," *Fluid Phase Equilib.*, **132**, 139 (1997).

Manuscript received Nov. 18, 1999, and revision received Apr. 20, 2000.